

Nanoscale

Accepted Manuscript



This is an *Accepted Manuscript*, which has been through the Royal Society of Chemistry peer review process and has been accepted for publication.

Accepted Manuscripts are published online shortly after acceptance, before technical editing, formatting and proof reading. Using this free service, authors can make their results available to the community, in citable form, before we publish the edited article. We will replace this *Accepted Manuscript* with the edited and formatted *Advance Article* as soon as it is available.

You can find more information about *Accepted Manuscripts* in the [Information for Authors](#).

Please note that technical editing may introduce minor changes to the text and/or graphics, which may alter content. The journal's standard [Terms & Conditions](#) and the [Ethical guidelines](#) still apply. In no event shall the Royal Society of Chemistry be held responsible for any errors or omissions in this *Accepted Manuscript* or any consequences arising from the use of any information it contains.

ARTICLE

Axially assembled photosynthetic reaction center mimics composed of tetrathiafulvalene, aluminum(III) porphyrin and fullerene entities

Cite this: DOI: 10.1039/x0xx00000x

Received 00th January 2012,
Accepted 00th January 2012

DOI: 10.1039/x0xx00000x

www.rsc.org/

Prashanth K. Poddutoori,^{*,a} Gary N. Lim,^b Atula S. D. Sandanayaka,^c Paul A. Karr,^d Osamu Ito,^e Francis D'Souza,^{*,b} Melanie Pilkington,^a Art van der Est^{*,a}

The distance dependence of sequential electron transfer has been studied in six, vertical, linear supramolecular triads, (TTF-Ph_n-py→AlPor-Ph_m-C₆₀, n = 0, 1 and m = 1, 2, 3), constructed using tetrathiafulvalene (TTF), aluminum(III) porphyrin (AlPor) and fullerene (C₆₀) entities. The C₆₀ and TTF units are bound to the Al center on opposite faces of the porphyrin; the C₆₀ through a covalent axial bond using a benzoate spacer, and the TTF through a coordination bond via an appended pyridine. Time-resolved optical and EPR spectroscopic methods and computational studies are used to demonstrate that excitation of the porphyrin leads to step-wise, sequential electron transfer (ET) between TTF and C₆₀, and to study the electron transfer rates and exchange coupling between the components of the triads as a function of the bridge lengths. Femtosecond transient absorption studies show that the rates of charge separation, k_{CS} are in the range of 10^9 - 10^{11} s⁻¹, depending on the length of the bridges. The lifetimes of the charge-separated state TTF^{•+}-C₆₀^{•-} obtained from transient absorbance experiments and the singlet lifetimes of the radical pairs obtained by time-resolved EPR are in good agreement with each other and range from 60-130 ns in the triads. The time-resolved EPR data also show that population of the triplet sublevels of the charge-separated state in the presence of a magnetic field leads to much longer lifetimes of >1 μs. The data show that a modest stabilization of the charge separation lifetime occurs in the triads. The attenuation factor $\beta = 0.36 \text{ \AA}^{-1}$ obtained from the exchange coupling values between TTF^{•+} and C₆₀^{•-} is consistent with values reported in the literature for oligophenylene bridged TTF-C₆₀ conjugates. The singlet charge recombination lifetime shows a much weaker dependence on the distance between the donor and acceptor, suggesting that a simple superexchange model is not sufficient to describe the back reaction.

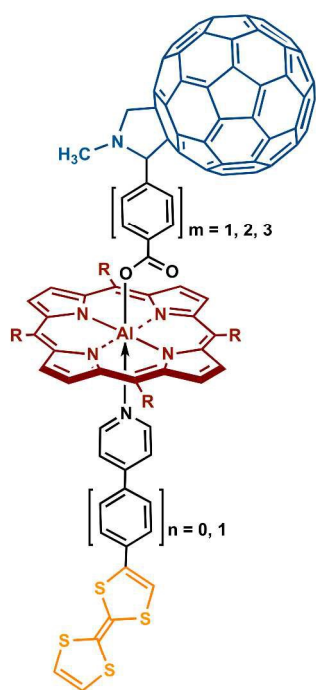
1. Introduction

In photosynthesis solar energy conversion is achieved by a multi-step electron transfer reaction in which the initial charge separation between chlorophyll and pheophytin (or between two chlorophyll molecules) is stabilized by a series of subsequent electron transfer steps that separate the two unpaired electrons.¹⁻⁵ Sequential electron transfer, as found in photosynthetic reaction centers, is a necessary design principle for achieving a high quantum yield of long-lived, light-induced charge separation because the initial electron transfer step must be fast enough to successfully compete with other decay processes that would otherwise lead to dissipation of the absorbed light energy. In a single donor-acceptor pair it is not possible to optimize forward electron transfer without increasing the rate of charge recombination. Thus, further

electron transfer steps are required to achieve long-lived charge separation. There are many reports of supramolecular complexes designed to perform light-induced charge separation⁶⁻¹⁵ but achieving highly efficient light-induced sequential electron transfer in such systems remains a significant challenge.^{8, 11, 16, 17}

Porphyrin (Por) derivatives are commonly used as both optical and redox active components in such complexes¹⁸⁻²² because their redox potentials and other properties can be easily tuned by changing substituents on the periphery and/or the element in the center of the Por ring and because they absorb light over a wide spectral range, which ensures more efficient use of the solar spectrum.^{23, 24} A crucial factor in the function of any electron transfer system is the electronic coupling between the donors and acceptors, which depends to a large extent on their spatial arrangement and whether the bonds between them

promote exchange coupling.²⁵ The influence of the length, bonding and conformation of the bridges have been studied in porphyrin-based systems in which the components are linked via bridges to the periphery of the Por ring.^{8, 11, 16, 26-30} However, there are fewer studies of these factors in complexes with the components linked axially via the central element of the Por ring.³¹⁻⁴³ In the natural reaction centers the chlorophylls are generally bound to the protein via axially ligation, often by histidine, and the axial ligands are important for controlling factors such as the free energy change and electronic coupling that govern electron transfer.⁴⁴ For artificial complexes, an added advantage of the axial arrangement is that the placement of the donor and acceptor units on opposite faces of the porphyrin ensures that they are spatially well separated and that unwanted interactions are minimized. This arrangement is difficult to achieve with transition metal porphyrins, which often only allow for coordination of one axial ligand, and attachment of two different ligands via coordination bonds, is difficult to control. Hence, examples of step-wise or cascade electron transfer in such systems remain extremely rare.^{45, 46}



- $n = 0, m = 1$: TTF-py \rightarrow AlPor-Ph-C₆₀
 $n = 1, m = 1$: TTF-Ph-py \rightarrow AlPor-Ph-C₆₀
 $n = 0, m = 2$: TTF-py \rightarrow AlPor-Ph₂-C₆₀
 $n = 1, m = 2$: TTF-Ph-py \rightarrow AlPor-Ph₂-C₆₀
 $n = 0, m = 3$: TTF-py \rightarrow AlPor-Ph₃-C₆₀
 $n = 1, m = 3$: TTF-Ph-py \rightarrow AlPor-Ph₃-C₆₀

Figure 1. Structures of the axial supramolecular triads investigated in this study.

The problem of attaching electron transfer components axially can be addressed by using porphyrins that contain main group elements at the center of the porphyrin ring. For example, aluminum(III) porphyrins (AlPors) form axial covalent bonds with alcohols, carboxylic acids and phosphinates resulting a 5-coordinate metal center.⁴⁵⁻⁵⁴ Moreover, the high Lewis acidity

of Al allows coordination by Lewis bases to form 6-coordinate complexes with the covalent ligand on one face of the porphyrin and the coordination bond on the opposite face. Recently, we reported examples of supramolecular triads in which a naphthalenediimide (NDI) derivative was attached covalently via an ester linkage and a bridging group to AlPor in the axial position and a tetrathiafulvalene (TTF) derivative was coordinated via a pyridine group to the opposite face of the porphyrin.⁵⁵ Optical and electron paramagnetic resonance (EPR) data showed that excitation of porphyrin leads to sequential, two-step electron transfer to generate the charge separated state TTF^{•+}-NDI^{•-}. However, the lifetime of the charge separation was short (<10 ns) unless a nematic liquid crystalline solvent was used. This observation suggests that the stabilization of the charge separation is limited by the reorganization energy.

In fullerene (C₆₀) derivatives delocalization of the charge over the C₆₀ dodecahedron stabilizes the unpaired electron and has been shown to result in low reorganization energy.⁵⁶⁻⁶¹ This combination of properties has led to a number of studies of reaction-center mimics based on Por and C₆₀ conjugates^{11, 16, 62-68} many of which perform sequential electron transfer.^{8, 11, 16, 26-30} We have previously reported on several triads in which C₆₀ was bound axially to AlPor and a secondary donor ferrocene (Fc) or phenothiazine (PTZ) was placed on the opposite face of the Por from the C₆₀.^{45, 46} These complexes undergo sequential electron transfer but the properties of Fc and PTZ are problematic. In the case PTZ the driving force for secondary electron transfer is very low and with Fc, the iron atom of Fc promotes fast recombination.

Here we report a series of new triads, in which the secondary donor is a tetrathiafulvalene (TTF) derivative, with the general formula TTF-Ph_n-py \rightarrow AlPor-Ph_m-C₆₀. The structures of the triads are shown in Figure 1. The optical and magnetic properties of the TTF^{•+} radical cation and C₆₀^{•-} radical anion make it possible to easily detect the formation and decay of TTF^{•+}-AlPor-C₆₀^{•-} by both transient absorption and transient EPR (TREPR) spectroscopy. Using this combination of techniques the kinetics and spin selectivity of the electron transfer and the electronic coupling within the complexes can be evaluated. We have studied the dependence of these properties on the donor-acceptor distance by varying the number of phenyl rings in the bridge between TTF and AlPor, and we show that there is an optimal length to the bridging groups for formation and stabilization TTF^{•+}-AlPor-C₆₀^{•-}. The stabilization of the charge separation by sequential electron transfer is relatively modest increasing the lifetime of C₆₀^{•-} from ~40 ns to ~100 ns. However, the transient EPR data indicate that in a magnetic field the back-reaction is strongly spin selective and the triplet lifetime of the secondary radical pair is at least an order of magnitude longer than the singlet lifetime.

2. Experimental Section

2.1 General. ^1H NMR spectra were recorded with a Bruker Avance 300 Digital NMR spectrometer using CDCl_3 , $(\text{CD}_3)_2\text{SO}$ and CD_3OD as the solvent. Mass spectra (Fast atom bombardment (FAB) and Matrix-assisted laser desorption/ionization time-of-flight (MALDI-TOF)) were recorded on a Kratos Concept 1S High Resolution E/B mass spectrometer and Bruker Autoflex TOF/MALDI-TOF spectrometer. The UV/VIS spectra were recorded with a ThermoSpectronic/Unicam UV-4 UV-VIS spectrometer. Steady-state emission spectra were recorded using a Photon Technologies International (London, Ontario) Quanta Master Model QM-2001 L-format, equipped with double-grating monochromators, a 150 W xenon lamp, running Felix 32 software. Cyclic and differential pulse voltammetric experiments were performed in *o*-dichlorobenzene (*o*-DCB) containing 0.1 M tetrabutylammoniumperchlorate (TBAP) on a BAS Epsilon electrochemical analyzer (working: glassy carbon, auxiliary electrodes: Pt wire; reference electrode: Ag). The Fc^+/Fc (Fc = ferrocene) couple was used to calibrate the redox potential values.

2.2 DFT Calculations. The geometry and electronic structures of the supramolecular assemblies were predicted by performing Density Functional Theory (DFT) calculations. The calculations were performed using Gaussian 09:AS64L-G09RevD.01⁶⁹ and all structures were constructed and visualized utilizing GaussView:5.0.9. The Becke Three Parameter Hybrid Functional utilizing the Lee-Yang-Parr non-local correlation expression (B3LYP) was chosen as the DFT method. Mixed split valence basis sets with polarizing Gaussians: 6-311G(d, p) (for H, N, C and O) and 6-311G(df) (Al and S) were used to complete the model chemistry. Structural models of all six triads were first constructed using GaussView. The initial structures were then up-loaded to a supercomputer housed at the Holland Computing Center and the geometry of each was optimized, *in-vacuo*, to a stationary point on a Born-Oppenheimer surface using the Gaussian 09 software suite and the functional and basis sets given above. Orbital diagrams and electrostatic potential maps of the optimized structure were then produced using GaussView and the formatted check files from the Gaussian 09 computation.

2.3 Absorption and Fluorescence Titrations. Absorption titrations were carried out in *o*-DCB at concentrations appropriate for measuring the Q band. A solution containing the acceptor ($\text{A} = \text{AlPor-Ph}$ or $\text{AlPor-Ph}_m\text{-C}_{60}$) was placed in a cuvette and titrated by adding aliquots of a concentrated solution of the donor ($\text{D} = \text{py}$, TTF-py or TTF-Ph-py). The donor solution also contained the acceptor at its initial concentration so that the porphyrin concentration remained constant throughout the titration. The binding constant (K) were calculated using the Benesi-Hildebrand equation,⁷⁰ details are shown in our previous papers.^{46, 55} In an analogous manner, steady-state fluorescence titrations were carried out in *o*-DCB using solutions at constant concentration of acceptor and varying concentration of donor. The solutions were excited at

the isobestic point wavelength, which was obtained from the absorption titrations.

2.4 Femtosecond Transient Absorption Spectroscopy. Femtosecond transient absorption spectroscopy experiments were performed using an Ultrafast Femtosecond Laser Source (Libra) by Coherent incorporating diode-pumped, mode locked Ti:Sapphire laser (Vitesse) and diode-pumped intra cavity doubled Nd:YLF laser (Evolution) to generate a compressed laser output of 1.45 W. For optical detection, a Helios transient absorption spectrometer coupled with femtosecond harmonics generator both provided by Ultrafast Systems LLC was used. The source for the pump and probe pulses were derived from the fundamental output of Libra (Compressed output 1.45 W, pulse width 100 fs) at a repetition rate of 1 kHz. 95% of the fundamental output of the laser was introduced into harmonic generator which produces second and third harmonics of 400 and 267 nm besides the fundamental 800 nm for excitation, while the rest of the output was used for generation of white light continuum. In the present study, the second harmonic 400 nm excitation pump was used in all the experiments. Kinetic traces at appropriate wavelengths were assembled from the time-resolved spectral data. Data analysis was performed using Surface Explorer software supplied by Ultrafast Systems. All measurements were conducted in degassed solutions at 298 K.

2.5 Nanosecond Transient Absorption Spectroscopy. Nanosecond transient absorption measurements were carried out in Ar saturated *o*-DCB using the second harmonic (532 nm) of a Nd:YAG laser (Spectra-Physics, Quanta-Ray GCR-130, 5 ns fwhm) as an excitation source. For transient absorption spectra in the near-IR region (600-1200 nm) and the time-profiles, monitoring light from a pulsed Xe lamp was detected with a Ge-APD (Hamamatsu Photonics, B2834). For the measurements in the visible region (400-1000 nm), a Si-PIN photodiode (Hamamatsu Photonics, S1722-02) was used as a detector.

2.6 Transient EPR Spectroscopy. Transient EPR time/field data sets were recorded using a modified Bruker EPR 200D-SRC X-band spectrometer (Bruker Canada, Milton ON, Canada). Light excitation at 532 nm was achieved using 10 ns pulses from a Nd:YAG laser at a repetition rate of 10 Hz. EPR samples were prepared by dissolving the porphyrin complex under study in *o*-DCB to a concentration of $\sim 10^{-4}$ M. The solutions were purged with N_2 and then placed in a sealed flat cell.

3. Results and Discussion

3.1 Synthesis. The details of the preparation and characterization of the components of the dyads and triads are given in the supporting information, Schemes S1 and S2. Briefly, the new dyads, $\text{AlPor-Ph}_2\text{-C}_{60}$ and $\text{AlPor-Ph}_3\text{-C}_{60}$, were prepared by condensation of tetraphenylporphyrinato-aluminum(III)hydroxide (AlPor-OH) with $\text{C}_{60}\text{-Ph}_2\text{-COOH}$ and $\text{C}_{60}\text{-Ph}_3\text{-COOH}$, respectively in quantitative yields, Scheme S3. Structural characterization of the newly synthesized dyads was

carried out with FAB-MS, NMR and absorption techniques. Synthesis and characterization of dyad AlPor-Ph-C₆₀ and reference porphyrin AlPor-Ph and also pyridine appended tetrathiafulvalene derivatives (TTF-py and TTF-Ph-py) have been reported elsewhere.^{45, 55} Scheme S4 shows the coordination of TTF-Ph_n-py (n = 0, 1) with AlPor-Ph_m-C₆₀ (m = 1, 2, 3) which affords the linear axial triads shown in Figure 1. Formation of the triads was monitored by NMR, UV-VIS absorption and steady-state fluorescence spectroscopy. Characteristic up field shifts of the pyridine protons in the NMR spectra (see supporting information Figure S5 & S6) confirm that coordination occurs via the pyridine group.

3.2 Characterization by UV-visible spectroscopy. The UV/vis absorption spectra of the components of the triads

measured are shown in Figure 2a and the data are summarized in Table S1. The AlPor unit absorbs between 375-700 nm with the characteristic intense Soret band at ~415 nm and weak Q-bands at ~550 nm and 580 nm. The functionalized C₆₀ derivatives (C₆₀-Ph₂-COOH, C₆₀-Ph₃-COOH) absorb in the ultra-violet region between 230-375 nm. There are noticeable differences in the ultra-violet region (270-360 nm) of the dyads, where the absorption is predominantly due to the phenyl ring. As expected, the absorbance between 270-360 nm increases as with number of the phenyl rings present in the dyads. The spectrum of the dyad is essentially a superposition of the spectra of the corresponding reference compounds. However, as reported previously⁴⁵ and as has been observed in related porphyrin-fullerene complexes,^{37, 71-73} the weak long-wavelength absorbance of AlPor-Ph-C₆₀ is stronger than that of

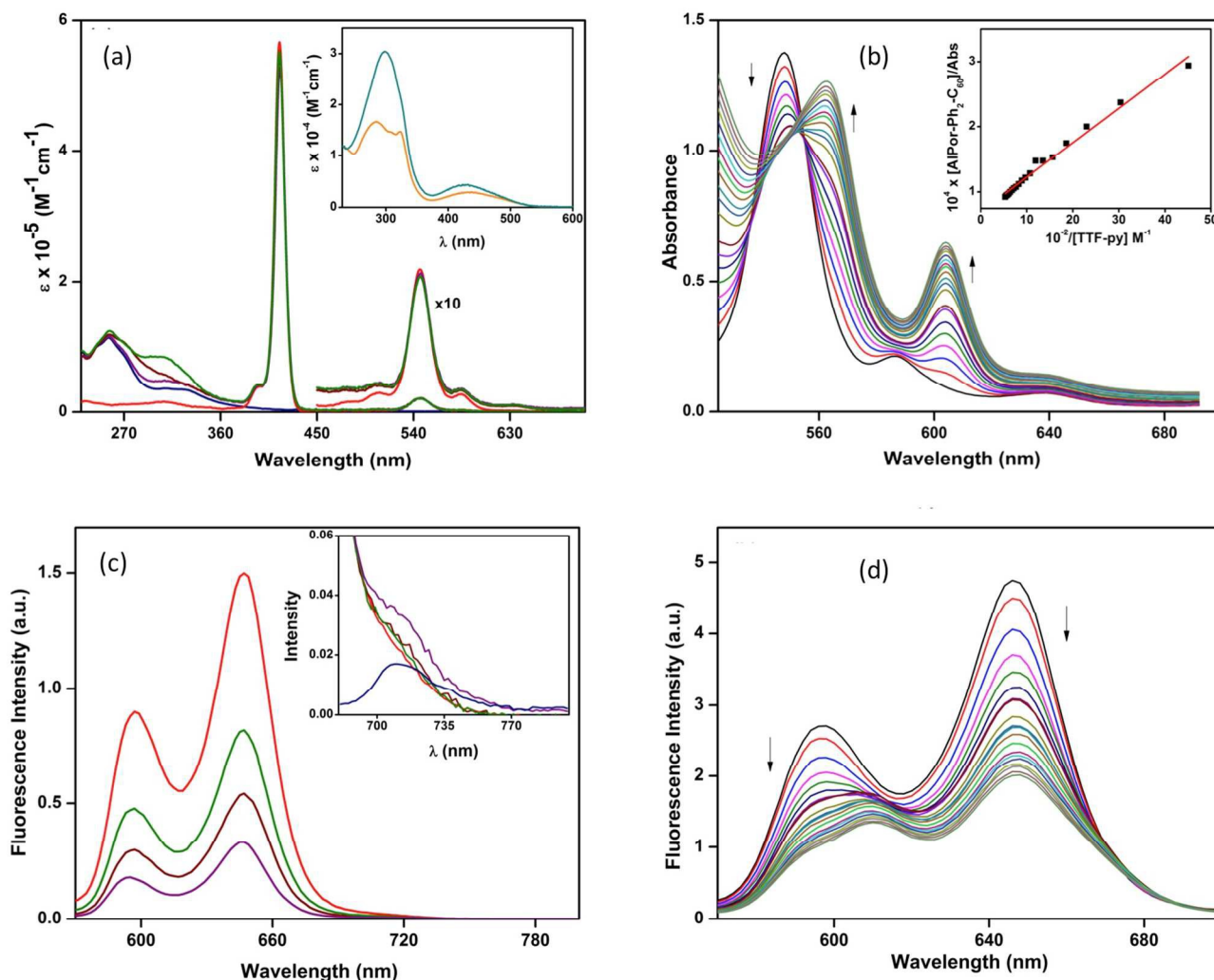


Figure 2. (a) UV-visible absorption spectra in dichloromethane. AlPor-Ph-C₆₀ (purple), AlPor-Ph₂-C₆₀ (maroon), AlPor-Ph₃-C₆₀ (green), AlPor-Ph (red) and C₆₀-Ph-COOH (blue); inset: TTF-py (orange) and TTF-Ph-py (cyan). The porphyrin Q bands and TTF bands were multiplied by factor of 10. (b) Absorption titrations of AlPor-Ph₂-C₆₀ with TTF-py in *o*-DCB. The inset shows the Benesi-Hildebrand plot of the absorbance change at 604 nm. Calculated binding constant $K = 1.2 \times 10^3 \text{ M}^{-1}$. (c) Fluorescence spectra of AlPor-Ph (red), AlPor-Ph-C₆₀ (purple), AlPor-Ph₂-C₆₀ (maroon) and AlPor-Ph₃-C₆₀ (green) in *o*-DCB. Excitation light wavelength 550 nm. (d) Fluorescence titrations of AlPor-Ph₂-C₆₀ with TTF-py in *o*-DCB. The excitation wavelength was chosen at the isosbestic point, 555 nm, obtained from UV-visible titrations. In titrations TTF-py was added up to $1.9 \times 10^{-3} \text{ M}$ in $10 \mu\text{l}$ ($1.12 \times 10^{-4} \text{ M}$) increments to a 1 ml ($6 \times 10^{-5} \text{ M}$) solution of AlPor-Ph₂-C₆₀.

AlPor-Ph, C₆₀COOMe, a 1:1 mixture of AlPor-Ph and C₆₀COOMe and dyads with longer bridging groups AlPor-Ph₂-

C₆₀ and AlPor-Ph₃-C₆₀ (see Figure S3). Overall, the spectra indicate that the porphyrin and fullerene units in AlPor-Ph_m-C₆₀

($m = 1-3$) do not interact strongly but the difference at longer wavelength suggests that a weak charge-transfer interaction, which decreases with increasing distance, may exist. The py-appended TTF derivatives, used to construct the self-assembled supramolecular triads, have relatively weak and very broad absorption bands (Figure 2a inset) at $\lambda = 304$ (average of 285 and 323 nm bands) and $\lambda = 432$ nm for TTF-py, and at $\lambda = 299$ and 427 nm for TTF-Ph-py.

Addition of TTF-Ph_n-py ($n = 0, 1$) to a solution of AlPor-Ph_m-C₆₀ ($m = 1-3$) results in significant changes in the wavelengths of the porphyrin Q-bands as a result of complex formation. Because the 432 nm band of TTF-Ph_n-py and AlPor Soret band at 416 nm overlap, the Q-bands were used to monitor the titrations, see Figure 2b and Figures S7, S8, S10, S12, S13. The observed shifts in the porphyrin bands are typical of axial coordination of nitrogen ligands to AlPors and confirm

the formation of supramolecular triads in the solutions. Similar absorption changes were observed from controlled titration experiments, i.e. py vs AlPor-Ph_m-C₆₀ ($m = 1-3$), py vs AlPor-Ph and TTF-Ph_n-py ($n = 0, 1$) vs AlPor-Ph, see supporting information Figures S9, S11, S14-S17. Figure 2b shows an absorbance titration of TTF-py against AlPor-Ph₂-C₆₀ from which a Benesi-Hildebrand plot (Figure 2b inset) can be constructed to obtain the binding constant. A value of $\sim(1.0-1.5) \times 10^3 \text{ M}^{-1}$ is obtained for all of the complexes (Table S1).

3.3 DFT calculations. Further, the geometry and electronic structures of the supramolecular assemblies were predicted by performing Density Functional Theory (DFT) calculations using the B3LYP functional and the 6-311G(d, p) (for H, N, C and O) and 6-311G(df) (Al and S) basis sets using Gaussian 09.⁶⁹ Figure 3a-f shows optimized structures on a Born-

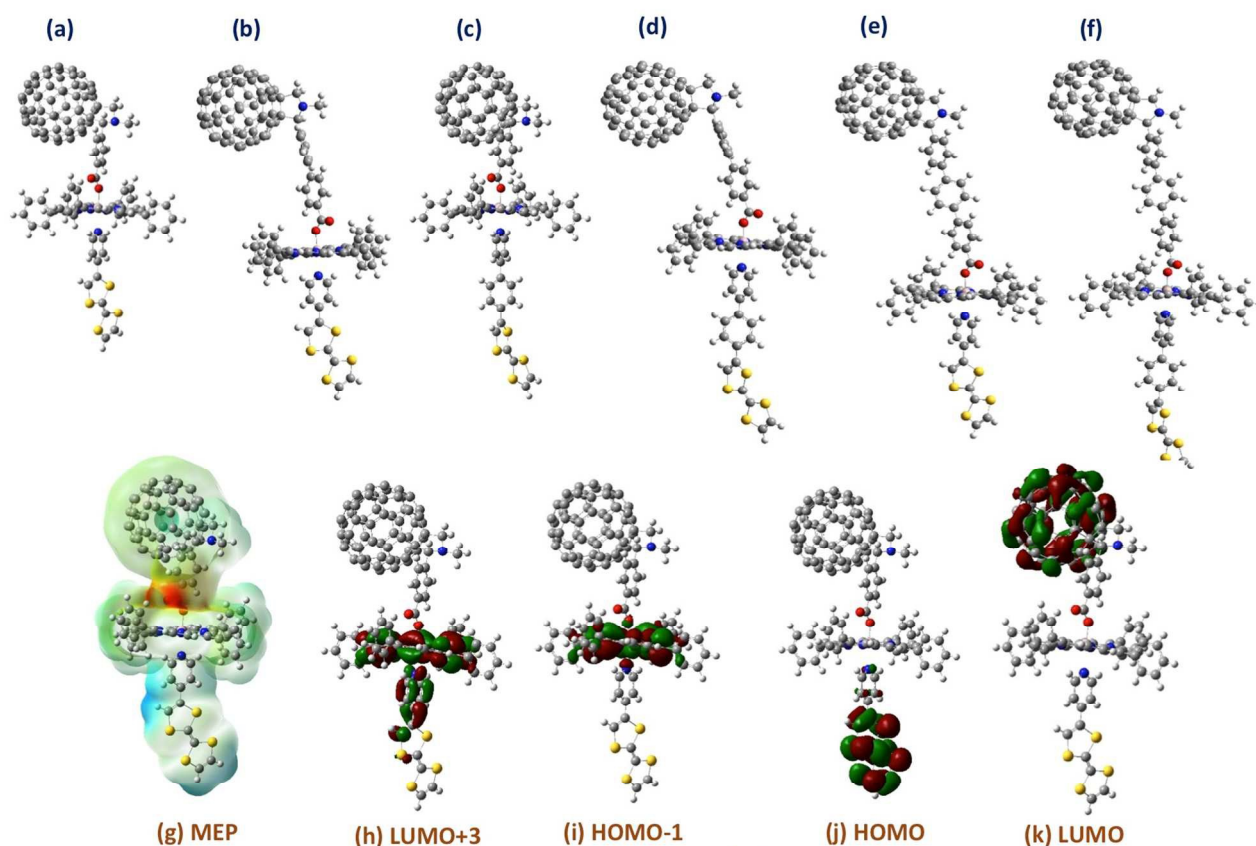


Figure 3. (a-f) Optimized structures of TTF-Ph_n-py→AlPor-Ph_m-C₆₀ ($n = 0, 1$ and $m = 1, 2, 3$). (g – k) Show the molecular electrostatic potential map (MEP), LUMO+3, HOMO-1, HOMO and LUMO of TTF-Ph-py→AlPor-Ph-C₆₀.

ARTICLE

Table 1. B3LYP/6-311G(d, p) (for H, N, C and O) and 6-311G(df) (Al and S) optimized edge-to-edge and center-to-center distances for the investigated series of dyads and triads.

Compound	Edge-to-edge distance, Å	Center-to-center distance, Å
AlPor-Ph-C ₆₀ ^a	9.65	11.73
TTF-py→AlPor-Ph-C ₆₀ ^b	14.18	20.36
TTF-Ph-py→AlPor-Ph-C ₆₀ ^b	18.02	24.22
AlPor-Ph ₂ -C ₆₀ ^a	11.96	15.38
TTF-py→AlPor-Ph ₂ -C ₆₀ ^b	17.90	24.13
TTF-Ph-py→AlPor-Ph ₂ -C ₆₀ ^b	21.22	27.96
AlPor-Ph ₃ -C ₆₀ ^a	16.42	19.87
TTF-py→AlPor-Ph ₃ -C ₆₀ ^b	22.64	29.17
TTF-Ph-py→AlPor-Ph ₃ -C ₆₀ ^b	26.66	33.34

^aDistance between AlPor and C₆₀. Edge-to-edge distance for dyad is measured from the nearest C₆₀ carbon to Al center. ^bDistance between TTF and C₆₀. TTF center is measured from the middle of C=C double bond. Edge-to-edge distance for triad is measured from the nearest C₆₀ carbon to the nearest TTF carbon.

Oppenheimer potential energy surface of the triads, TTF-Ph_n-py→AlPor-Ph_m-C₆₀ and the molecular electrostatic potential map revealing electron rich and deficient sites of the triad and the LUMO+3, HOMO-1, HOMO and LUMO are shown in Figure 3h-k (see Figures S19 - S21). These orbitals are localized on the AlPor, TTF and C₆₀ entities, respectively as expected. The calculated distances between the components of the triads (Table 1) show that the center-to-center distance between TTF and C₆₀ increases from 20.36 Å, with n = 0 and m = 1 to 33.34 Å, with n = 1 and m = 3. The optimized structures also provide the radii of AlPor, TTF and C₆₀ units, which are found to be 7.77 Å, 5.47 Å and 4.52 Å respectively.

3.4 Energy level diagram. The driving force for possible intramolecular electron transfer processes can be estimated using the optical data and redox potentials of the components of the triads. The redox potentials were determined from differential pulse voltammetry measurements in *o*-DCB with 0.1 M TBAP as the supporting electrolyte. Figure S22 shows the differential pulse voltammograms and the corresponding potentials are summarized in Table S1. The values given in Table S1 are relative to ferrocene, which has an oxidation potential of 0.74 V versus Ag wire in *o*-DCB with 0.1 M TBAP as the electrolyte in our experimental conditions. As seen in Table S1, the potentials of the first oxidation of TTF (~0.7 V), the first oxidation of AlPor (~1.1 V) and the first reduction of C₆₀ (~-0.44 V) do not vary significantly in any of the dyads, triads or reference compounds. Hence, as expected no significant perturbation of the molecular orbitals involved in the redox reactions occurs when the dyads and triads are formed. The energy level diagram derived from these data is shown in Figure 4. The energies of the lowest excited singlet state (E_S) and triplet state (E_T) of C₆₀ have been taken from the literature.^{46, 74} The singlet and triplet state energies of AlPor have been calculated from its optical absorption and emission

spectra, see Figure S23. The energies of the radical ion pair states are estimated the Weller equation⁷⁵:

$$E_{CS} = e \left[E_{1/2}(D^{*+}/D) - E_{1/2}(A/A^{*-}) \right] + G_S$$

where $E_{1/2}(D^{*+}/D)$ is the first oxidation potential of the donor, $E_{1/2}(A/A^{*-})$ is the first reduction potential of the acceptor. G_S is ion-pair stabilization and incorporates both the solvent-dependent Coulomb energy change upon ion-pair formation or recombination and the free energy of solvation of the ions,

$$G_S = \frac{e^2}{4\pi\epsilon_0} \left[\left(\frac{1}{2R_+} + \frac{1}{2R_-} - \frac{1}{R_{D-A}} \right) \frac{1}{\epsilon_S} - \left(\frac{1}{2R_+} + \frac{1}{2R_-} \right) \frac{1}{\epsilon_R} \right]$$

where R_+ , R_- and R_{D-A} are the donor radius, acceptor radius and center-to-center distance between the donor and acceptor, respectively. ϵ_S is the dielectric constant of the solvent used for the photophysical studies (2.38 and 9.93 for toluene and *o*-DCB, respectively). ϵ_R is the dielectric constant of the solvent used for measuring the redox potentials, in this case *o*-DCB. Note that the assumption of spherical charge distributions on the donor and acceptor and other limitations restrict the accuracy of the estimated energies to at best ± 0.1 eV⁷⁶

In the case of TTF-py→AlPor-Ph and TTF-Ph-py→AlPor-Ph, electron transfer from TTF to the excited singlet state of AlPor is exothermic with an estimated free energy change of approximately -0.43 eV (see Figure 4). However, whether this process can compete with intersystem crossing in the porphyrin depends on the activation barrier to electron transfer. Because the energy of the lowest excited triplet state of AlPor is lower than our estimate of the charge-separated state energy, triplet electron transfer is probably not feasible in TTF-py→AlPor-Ph and TTF-Ph-py→AlPor-Ph. In the TTF-Ph_n-py→AlPor-Ph_m-C₆₀ (n = 0, 1 and m = 1-3) triads, the sequential electron transfer reactions $\text{TTF}^{\cdot-} \text{AlPor}^* \text{C}_{60} \rightarrow \text{TTF}^{\cdot-} \text{AlPor}^{\cdot+} \text{C}_{60} \rightarrow \text{TTF}^{\cdot+} \text{AlPor} \text{C}_{60}^{\cdot-}$ and $\text{TTF}^{\cdot-} \text{AlPor}^* \text{C}_{60} \rightarrow \text{TTF}^{\cdot+} \text{AlPor}^{\cdot-} \text{C}_{60} \rightarrow \text{TTF}^{\cdot+} \text{AlPor} \text{C}_{60}^{\cdot-}$ are both energetically possible.

Triplet electron transfer from $^3\text{AlPor}^*$ to C_{60} is also energetically favourable but donation from TTF to $^3\text{AlPor}$ is not. Downhill triplet recombination is only feasible from $\text{TTF}^{+\bullet}\text{-AlPor}^-$. With toluene as the solvent, the radical ion-pairs are found to be higher in energy than in *o*-DCB (Figure S24) and the sequential electron transfer reactions remain exergonic. However, all of the calculated charge-separated states are higher in energy than the lowest excited triplet state of AlPor and C_{60} entities, which increases the possibility of triplet recombination.

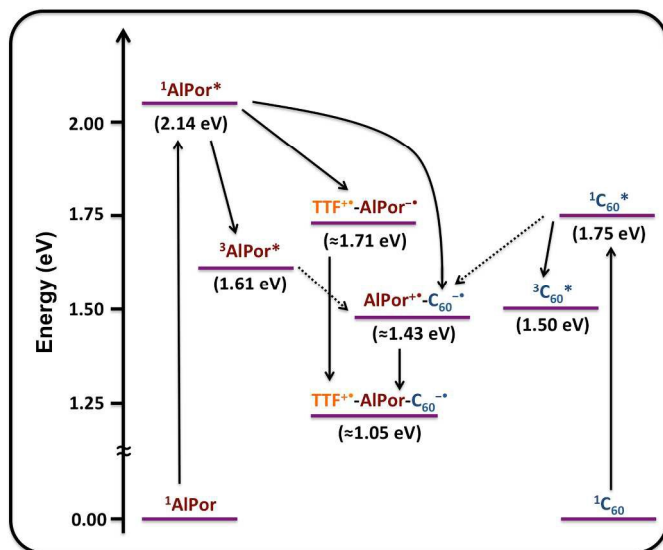


Figure 4. Energy level diagram illustrating the major photophysical processes in newly constructed dyads and triads in *o*-DCB.

3.5 Fluorescence Spectroscopy. Figure 2c shows the fluorescence spectra of the dyads, AlPor-Ph- C_{60} , AlPor-Ph₂- C_{60} and AlPor-Ph₃- C_{60} , and their reference monomer, AlPor-Ph in *o*-DCB. As discussed previously,^{45, 46} the fluorescence of AlPor is quenched (80%) in AlPor-Ph- C_{60} as a result of electron transfer from the excited singlet state ($^1\text{AlPor}^*$) to C_{60} . In the case of AlPor-Ph₂- C_{60} and AlPor-Ph₃- C_{60} , the AlPor fluorescence is also quenched but the quenching (66% and 50%, respectively) is lower than observed with AlPor-Ph- C_{60} . This suggests that the extra phenyl rings between the AlPor and C_{60} units decrease the electron transfer rate. As shown in the inset in Figure 2c, the 720 nm band due to fullerene fluorescence is very weak, hence little if any, energy transfer from $^1\text{AlPor}^*$ to C_{60} occurs.

Titration of AlPor-Ph with TTF-py in *o*-DCB, to form the dyad: TTF-py→AlPor-Ph also results in quenching of the AlPor fluorescence (Figure S15). To distinguish intramolecular and intermolecular quenching processes and to investigate possible quenching mechanisms several control experiments were carried out. When AlPor-Ph is titrated with TTF lacking the pyridine group so that it cannot coordinate to AlPor, no change in the fluorescence spectrum is observed (see Figure S18). Similarly, titration of AlPor-Ph (Figure S17) with pyridine leads primarily to a red shift of the fluorescence bands

with little change in intensity. Therefore, both the pyridine and TTF parts of the ligands are required to induce quenching of the fluorescence. From this, we conclude that an intramolecular process that causes radiationless decay of the porphyrin excited state occurs when the pyridine appended TTF unit binds to AlPor. Since the spectral overlap between AlPor emission and TTF absorption is weak, energy transfer from AlPor to TTF can be ruled out as an effective quenching mechanism. Hence, electron transfer (hole transfer) from TTF to $^1\text{AlPor}^*$ is proposed to be responsible for the quenching of AlPor fluorescence. The corresponding titration of AlPor-Ph with TTF-Ph-py to form TTF-Ph-py→AlPor-Ph (Figure S16) shows behavior that is intermediate between that in the titrations with pyridine and TTF-py. A clear red shift of the emission is observed, which is accompanied by some quenching. This implies that the phenyl group in the TTF unit slows the electron transfer as would be expected.

Upon addition of TTF-Ph_n-py (*n* = 0, 1) to the dyad (AlPor-Ph_m- C_{60} , *m* = 1-3), the fluorescence changes as a result of the formation of the supramolecular triads. Figure 2d shows the decrease in AlPor fluorescence with addition of TTF-py to AlPor-Ph₂- C_{60} and formation of triad TTF-py→AlPor-Ph₂- C_{60} . The decrease in fluorescence suggests that the rate of the proposed hole transfer from TTF to $^1\text{AlPor}^*$ is similar to or greater than the electron transfer rate to the C_{60} unit. Corresponding titrations for the other triads are shown in the supplementary information: TTF-py→AlPor-Ph- C_{60} (Figure S7), TTF-Ph-py→AlPor-Ph- C_{60} (Figure S8), TTF-Ph-py→AlPor-Ph₂- C_{60} (Figure S10), TTF-py→AlPor-Ph₃- C_{60} (Figure S12) and TTF-Ph-py→AlPor-Ph₃- C_{60} (Figure S13). The observed fluorescence changes in these triads can be explained by two factors: (1) hole transfer from TTF to AlPor* and (2) changes in the intrinsic fluorescence rates as a result of structural changes when py coordinates to Al. It is not possible to distinguish these two effects with certainty. However, a band shift and increase of the fluorescence is indicative of changes in the intrinsic fluorescence properties, whereas the proposed hole transfer from TTF is expected to quench the fluorescence. In all cases, the titrations with TTF-Ph-py (Figures S8, S10 and S13) show primarily a red shift of the fluorescence, while those with TTF-py (Figures 2d, S7 and S12) show quenching.

3.6 Femtosecond transient absorption studies (fs-TA).

Femtosecond (400 nm of 100 fs pulse width) pump-probe spectral studies were performed to confirm that photoinduced electron transfer occurs in the covalently linked dyads, AlPor-Ph_m- C_{60} , *m* = 1 - 3), and subsequent supramolecular triads, TTF-Ph_n-py→AlPor-Ph_m- C_{60} (*n* = 0, 1 and *m* = 1 - 3) and to investigate the kinetics of the light-induced processes. The studies were performed in both toluene and *o*-DCB. Although charge separation between TTF and C_{60} was clearly observed in both solvents, accurate values of the lifetimes were difficult to obtain in *o*-DCB. Because of the uncertainty in the lifetimes obtained in *o*-DCB, only the femtosecond pump-probe data obtained in toluene are discussed here. Formation of $\text{TTF}^{+\bullet}$ and $\text{C}_{60}^{\bullet-}$ is known to give absorbance increases in the range of 440-

600 nm⁵⁵ and 1000-1200 nm and weaker absorbance changes at 550-600 nm⁷⁷⁻⁸⁰ while formation ³C₆₀^{*} results in a strong peak at 700-720 nm.⁸¹ The triplet state of AlPor has a strong maximum at 500 nm and a weaker peak at 820 nm, while the small absorption changes due to AlPor⁺ are anticipated in the 600 - 650 nm region.^{45, 55} First, the features of fs transient absorption data of the reference compound AlPor-Ph were investigated. As shown in Figure S25, upon excitation, a broad absorption increase with a maximum at ~450 nm and a long tail stretching into the near IR is observed. Superimposed on the absorption increase are negative bands at 550 nm due to loss of the Q-band absorbance and at 590 and 650 nm due to emission from the S₁ state. The absorbance increase and Q-band bleach are formed instantaneously as a result of the S₀ → S_n transition. A kinetic phase with a lifetime of about 25 ps is then observed in the decay of the absorbance increase and the rise of the S₁ emission bands as the S_n state relaxes to the S₁ state. The decay of these bands is beyond the 3 ns time window of our instrument in accordance with the 7.88 ns lifetime of the S₁ state determined by time correlated single photon counting (TCSPC) fluorescence measurements in toluene (Figure S26). There is a shoulder at 487 at late times, which we tentatively assign to ³AlPor^{*}-Ph. Importantly, in the near-IR region, a peak at 1240 nm with the same decay profile as the singlet excited

state is observed, suggesting that this peak corresponds to excited singlet state absorption (See Figure S25b for time profiles). Such near-IR peaks corresponding to singlet-singlet transition have also been reported for other porphyrin derivatives.⁸²⁻⁸⁴ Next, the transient spectral features of AlPor-Ph_m-C₆₀, m = 1 - 3, were investigated (Figure 5a and b). Several features of the data provide evidence for the occurrence of photoinduced electron transfer from the ¹AlPor^{*} to C₆₀. First, the absorption peak at ~450 nm and the near-IR peak at 1240 nm, and the negative peaks due to S₁ emission at 590 and 650 nm decay more rapidly than in AlPor-Ph (see Figure 5d). The ¹AlPor^{*} decay is accompanied by a new band in the 1020 nm region corresponding to the formation of C₆₀^{-•}. In addition, broad absorbance in the 875-950 nm region was also observed indicating formation of ¹C₆₀^{*} either by direct excitation or energy transfer from ¹AlPor^{*}. The formation of AlPor⁺, expected to result in an absorption increase in the 600-650 nm region, was also observed, although overlapped with other peaks in this wavelength region. The fact that the 1020 nm peak of C₆₀^{-•} and 1240 nm peak of ¹AlPor^{*} are far from other transient bands allows them to be used to estimate the lifetimes of charge separation τ_{CS} and charge recombination, τ_{CR} . The time traces obtained at these wavelengths are shown in

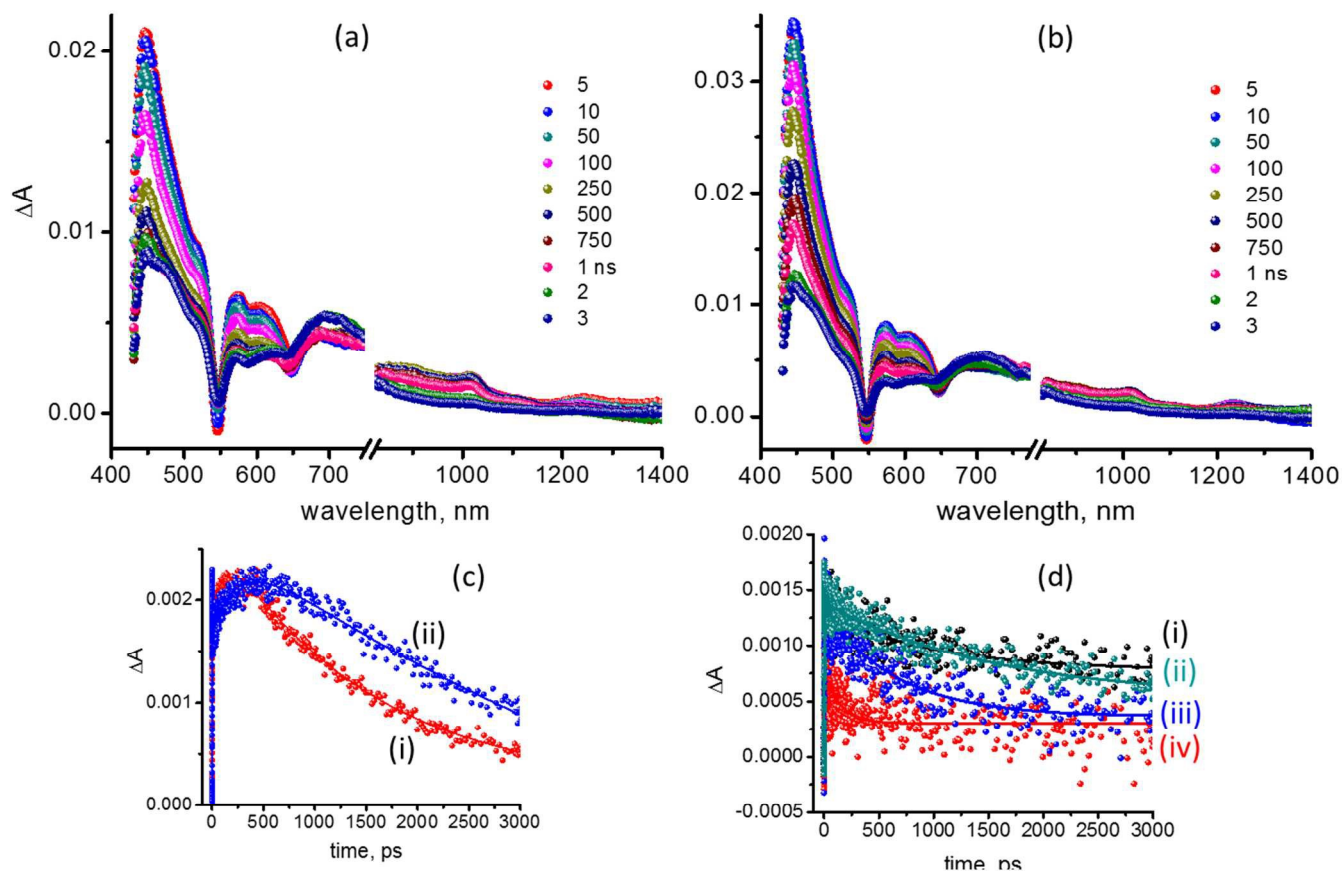


Figure 5. Femtosecond transient absorption spectra of (a) AlPor-Ph-C₆₀ and (b) AlPor-Ph₂-C₆₀ in toluene at the indicated time intervals. (c) The time profile of the 1000 nm radical anion peak of C₆₀ for (i) AlPor-Ph-C₆₀, and (ii) AlPor-Ph₂-C₆₀. (d) Normalized to the peak maxima decay of the 1240 nm peak of (i) AlPor-Ph, (ii) AlPor-Ph₂-C₆₀, (iii) AlPor-Ph₃-C₆₀, and (iv) AlPor-Ph-C₆₀.

ARTICLE

Figure 5c and d, respectively. As can be seen in Figure 5c, the rise time of the absorbance increase is clearly resolved allowing τ_{CS} to be determined, from which the rate of charge separation, k_{CS} can be calculated. The lifetime of the decay of the absorbance increase due to $^1\text{AlPor}^*$ at 1240 nm can also be used to calculate k_{CS} ($k_{CS} = 1/\tau_{\text{dyad}} - 1/\tau_{\text{ref}}$; where τ_{ref} is the lifetime of $^1\text{AlPor}^*\text{-Ph}$ being 7.88 ns in toluene, (see Figure 6d). The k_{CS} measured using these two approaches agree well, within the experimental error. However, the decay of $\text{C}_{60}^{\cdot-}$ is multiexponential with components that are longer than the 3 ns limit of the instrument (Figure 5c) which hampers the determination of τ_{CR} . The decay of the $\text{C}_{60}^{\cdot-}$ peak correlates with the decay of the Q-band bleaching at 550 nm showing that it corresponds to charge recombination to the ground state. In addition, a new absorption increase band is observed at 700 nm

corresponding to the formation of $^3\text{C}_{60}^*$. This band could be formed by charge recombination and/or by direct excitation and relaxation of C_{60} . The rise of the 700 nm band does not correlate directly with the decay of the 1020 nm band thus the $^3\text{C}_{60}^*$ state is probably populated by intersystem crossing. The values of \square_{CS} measured in toluene are presented in Table 2. As can be seen, the electron transfer to C_{60} occurs with a lifetime >100 ps and becomes slower as the length of the bridge to the porphyrin become longer, *i.e.* $\text{AlPor-Ph}_3\text{-C}_{60} > \text{AlPor-Ph}_2\text{-C}_{60} > \text{AlPor-Ph-C}_{60}$. The rate constants, k_{CS} , for the formation of $\text{AlPor}^+\text{-C}_{60}^{\cdot-}$ in toluene are also given in Table 2. These data show that, as expected, the rate of electron transfer in the dyads become slower as the distance between the donor and acceptor increase.

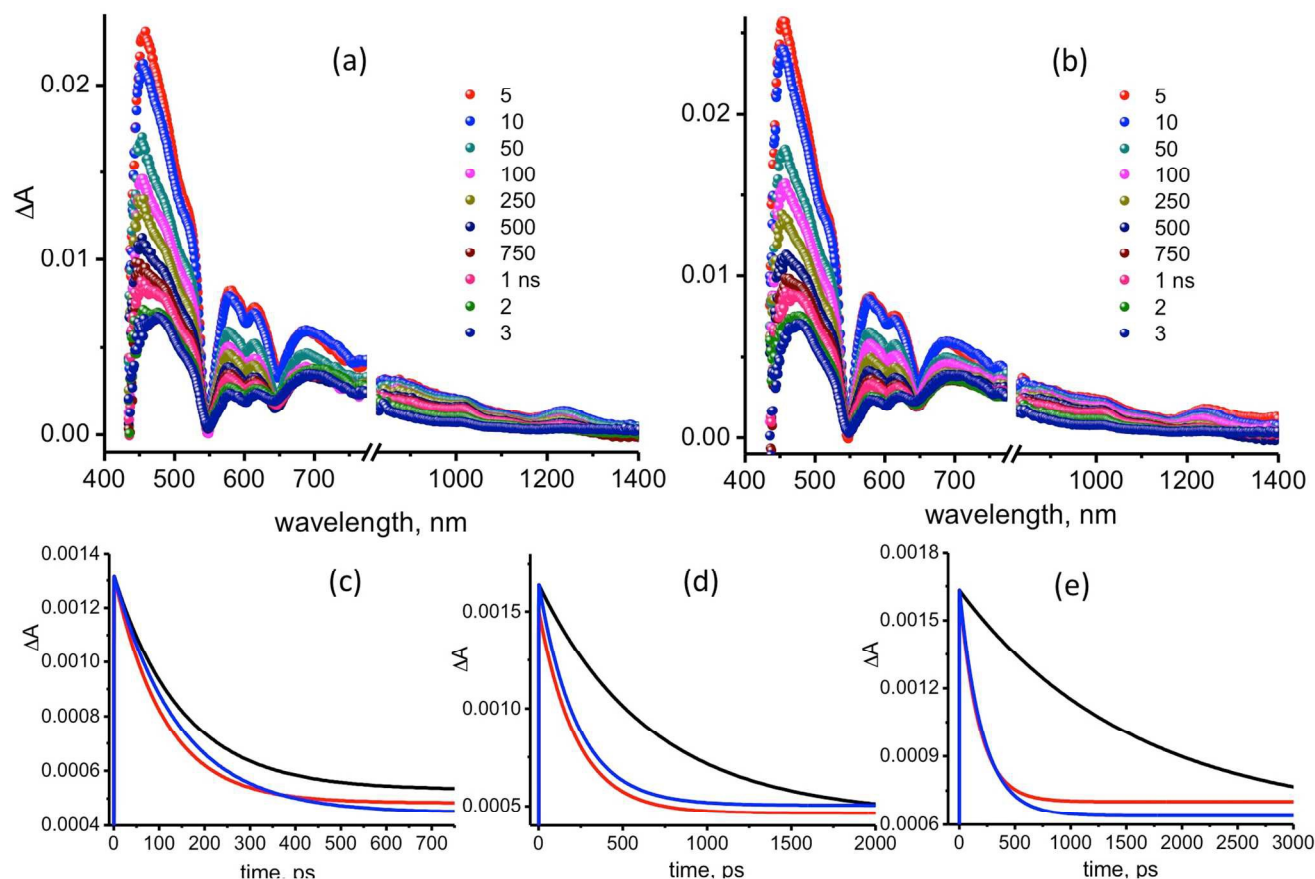


Figure 6. Femtosecond transient absorption spectra of (a) TTF-py \rightarrow AlPor-Ph₂-C₆₀ and (b) TTF-Ph-py \rightarrow AlPor-Ph₂-C₆₀ in toluene. The normalized to the peak maxima time profiles of the 1240 nm peak of $^1\text{AlPor}^*$ for the investigated AlPor-Ph-C₆₀, AlPor-Ph₂-C₆₀, and AlPor-Ph₃-C₆₀ dyads (black) in the presence of TTF-py (red) and TTF-Ph-py (blue) to form triads are shown in Figures c, d, and e, respectively. Note that the 1240 nm peak is too noisy due to rapid decay, for that reason only decay fit curves are shown

ARTICLE

Table 2. Charge separation and recombination lifetimes from *fs*- and *ns*-transient absorption and TREPR data. Parameters used to simulate the TREPR data.

Sample	<i>fs</i> -TA ^a		<i>ns</i> -TA ^c	TREPR ^d				
	τ_{CS} (ps)	k_{CS}^b ($\times 10^9 s^{-1}$)	τ_{CR} (ns)	τ_S (ns)	τ_T (μs)	$J(TTF^{+}C_{60}^{-})$ (mT)	Singlet character of early signal	Relative intensity of late signal
AlPor-Ph-C ₆₀	152	6.45	38	-	-	-	-	-
TTF-py→AlPor-Ph-C ₆₀	100	9.87	64	63	1.1	1.2	0.0	0.10
TTF-Ph-py→AlPor-Ph-C ₆₀	144	6.80	96	109	0.8	0.27	0.34	0.12
AlPor-Ph ₂ -C ₆₀	664	1.38	-	-	-	-	-	-
TTF-py→AlPor-Ph ₂ -C ₆₀	220	4.42	-	115	0.9	0.17	0.49	0.15
TTF-Ph-py→AlPor-Ph ₂ -C ₆₀	315	3.05	-	131	1.0	0.10	0.73	0.15
AlPor-Ph ₃ -C ₆₀	1620	0.49	-	-	-	-	-	-
TTF-py→AlPor-Ph ₃ -C ₆₀	196	4.97	-	-	-	-	-	-
TTF-Ph-py→AlPor-Ph ₃ -C ₆₀	330	2.91	-	-	-	-	-	-

^aIn Ar-saturated toluene. ^b $k_{CS} = 1/\tau_{dyad} - 1/\tau_{ref}$; where τ_{ref} is the lifetime of ¹AlPor* being 7.88 ns in toluene, here the τ values are decay constants of the 1240 nm peak corresponding to singlet-singlet transition of AlPor. ^{c,d}In Ar-saturated *o*-DCB. τ_S and τ_T are the singlet and triplet recombination lifetimes, respectively.

The supramolecular triads, TTF-Ph_n-py→AlPor-Ph_m-C₆₀, formed by coordinating TTF-Ph_n-py to AlPor-Ph_m-C₆₀ show evidence of sequential electron transfer (Figure 6, Table 2). First, as seen from the decay profiles of C₆₀^{•-} at 1020 nm, the radical ion-pairs persisted beyond the 3 ns time limit of the spectrometer. The absorption increase band between 450 and 500 nm becomes broader, suggesting the presence of the TTF^{•+} radical cation, which shows a peak at 480 nm when formed by electrochemical oxidation of TTF.⁵⁵ Additionally, the broad peak of AlPor^{•+} in the 600 nm range vanishes upon addition of TTF-py suggesting occurrence of a hole shift process (See Figure S27). Interestingly, the k_{CS} measured by monitoring the time profile of the near-IR peaks revealed faster charge separation than observed in the corresponding AlPor-Ph_m-C₆₀ dyads (see Figure 6c-e for time profiles and Table 2). For each series of triads with the same AlPor-C₆₀ bridge, the TTF-py adduct had the highest rate of charge separation, *i.e.* the following trend was observed: AlPor-Ph_m-C₆₀ < TTF-py→AlPor-Ph_m-C₆₀ > TTF-Ph-py→AlPor-Ph_m-C₆₀ (Table 2). Additionally, in the case of AlPor-Ph_m-C₆₀ dyads, charge recombination results in population of ³C₆₀^{•*} in toluene likely due to contributions from ¹C₆₀^{•*} generated either by direct excitation or energy transfer from ¹AlPor*.

As can be seen in Figures 5 and 6, the decay of the absorbance change at 1020 nm extends beyond the 3 ns limit of the fs transient absorption setup. Thus, we have also carried out nanosecond transient absorption measurements to study the long-lived charge separation.

3.7 Nanosecond Transient Absorption Spectroscopy (ns-TA).

Figure 7 shows the nanosecond transient absorption difference spectra of the triad, TTF-py→AlPor-Ph-C₆₀ measured in Ar-

saturated *o*-DCB solution at room temperature using 532-nm laser light to excite mainly the porphyrin unit. The characteristic peak due to C₆₀^{•-} is clearly visible at 1020 nm. The time profile at 1020 nm for TTF-py→AlPor-Ph-C₆₀, shown as an inset in Figure 8, decays to zero within about 400 ns and a fit of the transient yields a first-order rate constant of $1.57 \times 10^7 s^{-1}$ for the decay of C₆₀^{•-}. The same decay constant is also observed in the decay trace at 470 nm, where the absorbance increase due to TTF^{•+} is expected. A slightly lower rate of $1.0 \times 10^7 s^{-1}$ is obtained from the corresponding traces for TTF-Ph-py→AlPor-Ph-C₆₀, Figure S28. These rate constants are smaller by a factor of about three than the corresponding rate constant of $3 \times 10^7 s^{-1}$ obtained for py→AlPor-Ph-C₆₀ and AlPor-Ph-C₆₀.^{45, 46} and suggest that the initial charge separation (AlPor^{•+}-C₆₀^{•-}) is followed by a hole-shift from AlPor^{•+} to TTF to give the final charge-separated states, TTF^{•+}-py→AlPor-Ph-C₆₀^{•-} and TTF^{•+}-Ph-py→AlPor-Ph-C₆₀^{•-} in the two triads. These states are sufficiently long lived that they are detectable by transient EPR, which allows the spin selectivity of the electron transfer to be studied.

3.8 Time-Resolved EPR Spectroscopy (TREPR). Figure 8 shows the room temperature spin-polarized EPR spectra of four of the triads in *o*-DCB at two different times after the laser flash. The spectra on the left of the figure were extracted from the full dataset in a time window centered at 75 ns after the laser flash and those on the right are at 550 ns. Positive peaks represent absorption (A) and negative peaks are in emission (E). The spectrum of TTF-py→AlPor-Ph-C₆₀ at early time (Figure 8, top left) is the narrow A/E pattern typical of a moderately strongly coupled radical pair with predominant population of the T₀ level. The absorptive shoulder on the right hand end of the spectrum is due to a molecular triplet state,

ARTICLE

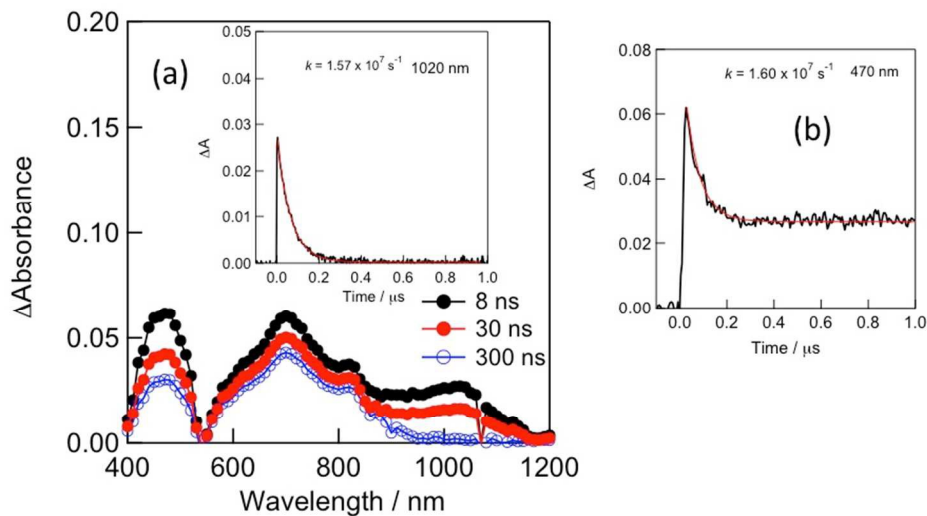


Figure 7. (a) Nanosecond transient absorption spectra of 0.1 mM TTF-py \rightarrow AlPor-Ph-C₆₀ observed by 532 nm (ca. 3 mJ/pulse) laser irradiation in *o*-DCB. Inset: Absorption time profile at 1020 nm. (b) Absorption time profile at 470 nm.

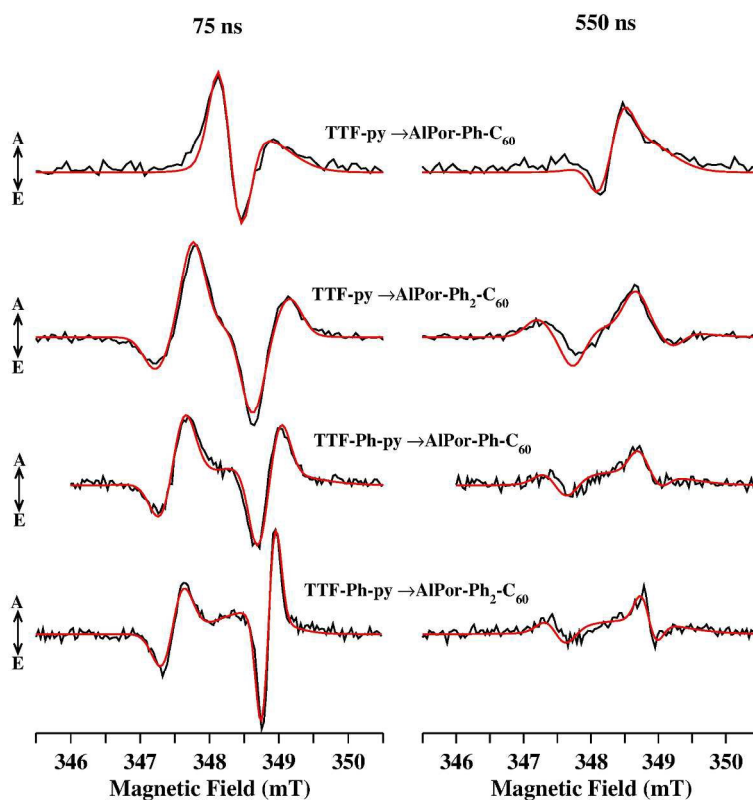


Figure 8. Room temperature spin-polarized transient EPR spectra of the TTF-Ph_n-py \rightarrow AlPor-Ph_m-C₆₀ triads. The spectra on the right and left have been extracted from the time/field data sets in time windows centered at 75 and 550 ns, respectively. The black traces are experimental spectra, and the red traces are simulations. The details of the simulations are given in the text.

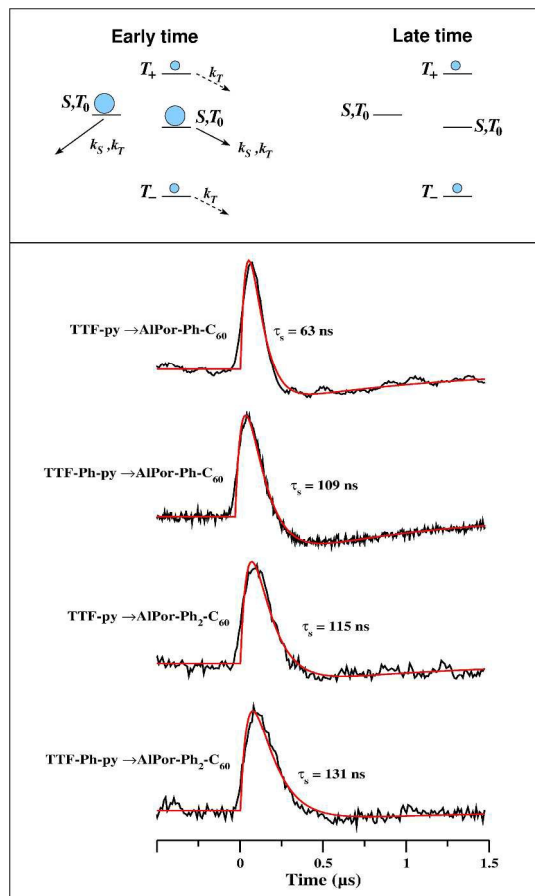


Figure 9. Time evolution of the population distribution of the radical pair spin states and the spin-polarized transient EPR signals. Top: qualitative diagram showing the time evolution of the population distribution of the spin states of the weakly coupled radical pair $\text{TTF}^+\text{C}_{60}^-$. Bottom: time traces of the spin-polarized EPR signal at the maximum of the absorptive signal near 347.4 mT. The black traces are the experimental data. The red traces are fits. The lifetime of the initial decay is indicated next to each trace.

probably $^3\text{C}_{60}$. The other three triads all show the E/A/E/A pattern of a weakly coupled radical pair. The low-field E/A doublet has a g-value of 2.0084 can be assigned to transitions associated with the TTF^+ radical cation, while the high-field doublet has a g-value of 2.0006 and is from the C_{60}^- radical anion. As expected the splitting of the doublets decreases as the distance between the two radicals increases. The linewidths of the peaks associated with C_{60}^- are expected to be narrower than those of TTF^+ because of the lack of unresolved hyperfine couplings in the fullerene. This effect is clearly seen in the spectrum of $\text{TTF-Ph-py} \rightarrow \text{AlPor-Ph}_2\text{-C}_{60}$ (Figure 8, bottom left). For the other triads, mixing of the spin states and/or a distribution of values for the spin-spin coupling results in

broader lines and roughly the same width for all four peaks. At later times the polarization patterns all become weaker and invert as a result of spin-selective recombination from the states with singlet character. This leaves population only in the two states (T_+ and T_-) with pure triplet character. This evolution of the population distribution is illustrated in the top of Figure 9. In the bottom part of Figure 9, transients from the four triads taken at the field position of the maximum absorptive TTF^{++} signal are shown. The singlet recombination of the radical pair leads to inversion of the signal from absorptive at early time to emissive at late time. The decay of the emissive polarization is due to a combination of spin relaxation and triplet recombination. The four transients in Figure 9 have been fitted with a kinetic model, which yields the singlet recombination lifetimes shown in Table 2 and as can be seen in the table these lifetimes agrees well with those obtained from the ns transient absorbance measurements. The fact that the decay of the late signal is roughly the same in all of the samples suggests that it is primarily due to spin relaxation.

The spin polarization patterns of light-induced radical pairs such as those in Figure 8 are determined by the population distribution of the spin states and they depend on the nature of the precursor to the radical pair. For a precursor in a pure singlet state, each radical has two peaks of equal intensity and

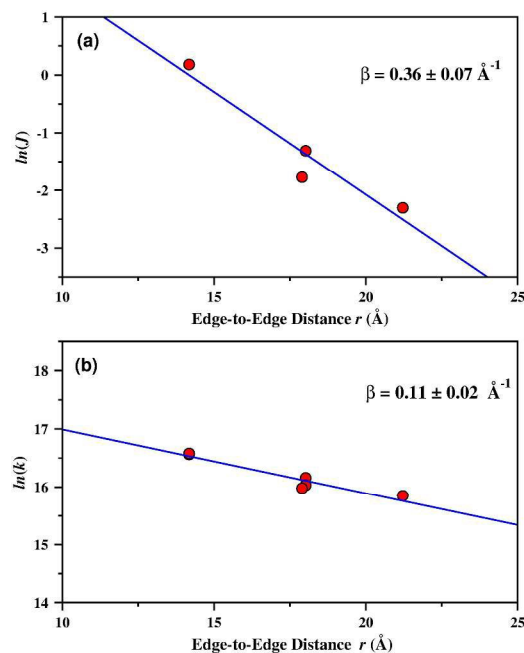


Figure 10. Distance dependence of the exchange coupling and back reaction rate. (a) exchange coupling from the simulations of the TREPR spectra. (b) back reaction rate from nanosecond transient absorbance and singlet recombination rate from TREPR data.

opposite polarization. The sign of the polarization E/A or A/E depends on the sign of the spin-spin coupling. If the precursor has triplet character one of the two lines for each radical will be stronger, *i.e.* the radical will acquire net polarization. Such triplet character can arise either from mixing of the S and T_0 during the lifetime of a radical pair precursor, or if the electron transfer is initiated from an excited triplet state. The red lines in the Figure 9 are simulations in which it has been assumed that the spin states are populated according to a mixture of their singlet and triplet characters. For the early spectra the amount of these two contributions varies and sign of the triplet-character contribution indicates predominant population of T_0 . For the late spectra the singlet contribution is zero and the sign of the triplet character correspond to population of only T_+ and T_- . A contribution from the spectrum of the C_{60} triplet state is also included as an absorptive Gaussian lineshape. The exchange coupling and weighting factors of the singlet and triplet contributions used in the simulations are given in Table 2. As can be seen, the exchange coupling between the radicals decreases as the distance between the two electrons increases. The coupling is expected to follow the relationship $J = J_0 \exp(-\beta(r-r_0))$. From a plot of $\ln(J)$ versus r (Figure 10a) we obtain a value of $\beta = 0.36 \pm 0.07 \text{ \AA}^{-1}$. This value is within error the same as that obtained for *p*-phenylene bridged biradicals⁸⁵ and porphyrins.⁸⁶ In contrast, *p*-phenyleneethynylene-bridged C_{60} -TTF dyads⁸⁷ and thiophene-bridged radicals⁸⁵ have values of β that are about a factor of two smaller. If the back reaction occurs by a superexchange mechanism then the rate should follow the same distance dependence as the exchange coupling, *i.e.* $k = k_0 \exp(-\beta(r-r_0))$. As shown in Figure 10b, a plot of $\ln k$ vs r is linear but the distance dependence of the recombination is much weaker. Weak distance dependence of electron transfer rates is often given as evidence for an incoherent hopping mechanism.²⁵ However, for the backreaction observed here, such a mechanism is unlikely because it would involve uphill electron transfer. Thus, the distance dependence of the backreaction does not appear to be governed by the superexchange mechanism but is difficult to rationalize in terms of a hopping mechanism.

For the two triads TTF-py→AlPor-Ph₃-C₆₀ and TTF-Ph-py→AlPor-Ph₃-C₆₀ transient EPR signals were not detectable at room temperature in *o*-DCB, while the shorter triads gave the spectra shown in Figure 8. The distance dependence of the exchange coupling provides a possible explanation of why this is so. From the plot in Figure 10a we estimate values of 0.05 and 0.01 mT for the exchange coupling in TTF-py→AlPor-Ph₃-C₆₀ and TTF-Ph-py→AlPor-Ph₃-C₆₀, respectively, based on the predicted distances between the radicals. The antiphase doublets of a weakly coupled radical pair arise from the overlap of two oppositely polarized, inhomogeneously broadened lines. The intensity of the spectrum is determined by the overlap of the two lines. If the inhomogeneous linewidth is larger than the spin-spin coupling the degree of overlap and the intensity are proportional to the spin-spin coupling.⁸⁸ Thus, the intensity of

the spectra for the two longest triads should be roughly one half and one tenth as intense as that of TTF-Ph-py→AlPor-Ph₂-C₆₀. Such a reduction in intensity would render the signals very weak but nonetheless detectable. Hence we can surmise that there is probably also some reduction in the quantum yield of TTF⁺-C₆₀⁻.

The initial singlet character of the TTF⁺-C₆₀⁻ radical pair shown in Table 2 also provides insight into the spin selectivity of the electron transfer. As can be seen the singlet character increases as the distance between the two radicals increases. This is not expected since the lifetime of the primary radical pair should increase and hence greater singlet-triplet mixing should occur as the bridge length increases. However, the fs-transient absorbance data show that a significant amount of singlet charge recombination to the ground state occurs on the timescale of ~1 ns. The singlet character of the transient EPR can be rationalized as the result of a decrease in the relative amount of this recombination as the bridge length is increased. Finally, the relative intensity of the late signal is a measure of the fraction of electron transfer originating from either ³AlPor or ³C₆₀. As can be seen in Table 2, this fraction is small and does not depend strongly on the structure of the triad.

4. Conclusions

The data presented here show that the use of the main group element Al in the porphyrin provides a convenient way of constructing donor acceptor triads. The small reorganization energy of C₆₀ leads to a significant increase in the stability of the final radical pair state compared to similar triads with naphthenediimide as the acceptor.⁵⁵ The data also illustrate the complementary nature of optical and TREPR measurements and the importance of the spin selectivity of the electron transfer. The weak distance dependence of the back reaction of the final radical pair and the significant levels of singlet recombination in the primary radical pair both suggest that further improvement of the yield and stability of the charge separation may be attainable by optimization of the bridge.

Acknowledgements

This work was supported by Discovery Grants from the Natural Sciences and Engineering Council of Canada to AvdE and MP and by the National Science Foundation (Grant No. 1401188 to FD). The computational work was completed utilizing the Holland Computing Center of the University of Nebraska.

Notes and references

^aDepartment of Chemistry, Brock University, 500 Glenridge Ave., St.Catharines, Ontario, Canada L2S 3A1. Email: ppoddutoori@brocku.ca; avde@brocku.ca.

^bDepartment of Chemistry, University of North Texas, 11555 Union Circle, 305070, Denton, TX 76203-5017, USA. E-mail: francis.dsouza@unt.edu.

^cSchool of Materials Science, Japan Advanced Institute of Science and Technology, Asahidai, Nomi, 923-1292, Japan.

- ^dDepartment of Physical Sciences and Mathematics, Wayne State College, 111 Main Street, Wayne, Nebraska, 68787, USA.
- ^fIMRAM, Tohoku University, Katahira, Sendai, 980-8577 Japan.
- [†] Electronic Supplementary Information (ESI) available: Synthesis details, NMR and absorption spectra, titrations (NMR, absorption and fluorescence), DFT calculations, differential pulse voltammetry, optical spectra of AlPor-Ph for singlet and triplet energy calculations, AlPor-Ph fluorescence decay curve and transient absorption spectra. See DOI: 10.1039/b000000x/
- J. Deisenhofer, O. Epp, K. Miki, R. Huber and H. Michel, *J. Mol. Biol.*, 1984, 180, 385-398.
 - J. Barber and B. Andersson, *Nature*, 1994, 370, 31-34.
 - J. Deisenhofer, Norris, J. R., ed., *The Photosynthetic Reaction Center*, Academic Press, San Diego, CA, 1993.
 - N. Krauss, W. D. Schubert, O. Klukas, P. Fromme, H. T. Witt and W. Saenger, *Nat. Struct. Biol.*, 1996, 3, 965-973.
 - P. Fromme, *Curr. Opin. Struct. Biol.*, 1996, 6, 473-484.
 - M. R. Wasielewski, *Acc. Chem. Res.*, 2009, 42, 1910-1921.
 - P. V. Kamat, *J. Phys. Chem. C*, 2007, 111, 2834-2860.
 - H. Imahori, Y. Mori and Y. Matano, *J. Photochem. Photobiol. C-Photochem. Rev.*, 2003, 4, 51-83.
 - J. Y. Liu, M. E. El-Khouly, S. Fukuzumi and D. K. P. Ng, *Chem.-Eur. J.*, 2011, 17, 1605-1613.
 - M. R. Wasielewski, *J. Org. Chem.*, 2006, 71, 5051-5066.
 - D. M. Guldi, *Chem. Soc. Rev.*, 2002, 31, 22-36.
 - D. Gust, T. A. Moore and A. L. Moore, *Acc. Chem. Res.*, 2001, 34, 40-48.
 - D. Gust and T. A. Moore, *Top. Curr. Chem.*, 1991, 159, 103-151.
 - A. Harriman and J. P. Sauvage, *Chem. Soc. Rev.*, 1996, 25, 41-&.
 - S. Fukuzumi, *Phys. Chem. Chem. Phys.*, 2008, 10, 2283-2297.
 - H. Imahori, *Org. Biomol. Chem.*, 2004, 2, 1425-1433.
 - M. Schmittel, R. S. K. Kishore and J. W. Bats, *Org. Biomol. Chem.*, 2007, 5, 78-86.
 - N. Aratani, D. Kim and A. Osuka, *Acc. Chem. Res.*, 2009, 42, 1922-1934.
 - I. Beletskaya, V. S. Tyurin, A. Y. Tsvadze, R. Guillard and C. Stern, *Chem. Rev.*, 2009, 109, 1659-1713.
 - H. Imahori, *J. Phys. Chem. B*, 2004, 108, 6130-6143.
 - Y. Kobuke and K. Ogawa, *Bull. Chem. Soc. Jpn.*, 2003, 76, 689-708.
 - S. L. Gould, G. Kodis, R. E. Palacios, L. de la Garza, A. Brune, D. Gust, T. A. Moore and A. L. Moore, *J. Phys. Chem. B*, 2004, 108, 10566-10580.
 - K. M. S. a. R. G. K. M. Kadish, ed., *The Porphyrin Handbook*, Academic Press, San Diego, 2000.
 - K. M. S. a. R. G. K. M. Kadish, ed., *Handbook of Porphyrin Science*, World Scientific, Singapore, 2010.
 - C. Schubert, J. Margraf, T. Clark and D. Guldi, *Chem. Soc. Rev.*, 2015.
 - H. Imahori, D. M. Guldi, K. Tamaki, Y. Yoshida, C. P. Luo, Y. Sakata and S. Fukuzumi, *J. Am. Chem. Soc.*, 2001, 123, 6617-6628.
 - M. Di Valentin, A. Bisol, G. Agostini, P. A. Liddell, G. Kodis, A. L. Moore, T. A. Moore, D. Gust and D. Carbonera, *J. Phys. Chem. B*, 2005, 109, 14401-14409.
 - D. Curiel, K. Ohkubo, J. R. Reimers, S. Fukuzumi and M. J. Crossley, *Phys. Chem. Chem. Phys.*, 2007, 9, 5260-5266.
 - P. A. Liddell, G. Kodis, L. de la Garza, J. L. Bahr, A. L. Moore, T. A. Moore and D. Gust, *Helv. Chim. Acta*, 2001, 84, 2765-2783.
 - G. Kodis, P. A. Liddell, L. de la Garza, A. L. Moore, T. A. Moore and D. Gust, *J. Mater. Chem.*, 2002, 12, 2100-2108.
 - F. D'Souza and O. Ito, *Chem. Commun.*, 2009, 4913-4928.
 - M. A. Fazio, A. Durandin, N. V. Tkachenko, M. Niemi, H. Lemmetyinen and D. I. Schuster, *Chem.-Eur. J.*, 2009, 15, 7698-7705.
 - S. Fukuzumi, T. Honda, K. Ohkubo and T. Kojima, *Dalton Trans.*, 2009, DOI: 10.1039/b901191a, 3880-3889.
 - H. J. Kim, K. M. Park, T. K. Ahn, S. K. Kim, K. S. Kim, D. H. Kim and H. J. Kim, *Chem. Commun.*, 2004, DOI: 10.1039/b411482c, 2594-2595.
 - T. Kojima, K. Hanabusa, K. Ohkubo, M. Shiro and S. Fukuzumi, *Chem.-Eur. J.*, 2010, 16, 3646-3655.
 - A. Trabolzi, M. Elhabiri, M. Urbani, J. L. D. de la Cruz, F. Ajamaa, N. Solladie, A. M. Albrecht-Gary and J. F. Nierengarten, *Chem. Commun.*, 2005, DOI: 10.1039/b510782b, 5736-5738.
 - F. D'Souza, E. Maligaspe, P. A. Karr, A. L. Schumacher, M. El Ojaimi, C. P. Gros, J. M. Barbe, K. Ohkubo and S. Fukuzumi, *Chem.-Eur. J.*, 2008, 14, 674-681.
 - M. E. El-Khouly, O. Ito, P. M. Smith and F. D'Souza, *J. Photochem. Photobiol. C-Photochem. Rev.*, 2004, 5, 79-104.
 - T. Da Ros, M. Prato, D. Guldi, E. Alessio, M. Ruzzi and L. Pasimeni, *Chem. Commun.*, 1999, 635-636.
 - F. D'Souza and O. Ito, *Coord. Chem. Rev.*, 2005, 249, 1410-1422.
 - F. D'Souza, G. R. Deviprasad, M. E. El-Khouly, M. Fujitsuka and O. Ito, *J. Am. Chem. Soc.*, 2001, 123, 5277-5284.
 - S. R. Wilson, S. MacMahon, F. T. Tat, P. D. Jarowski and D. I. Schuster, *Chem. Commun.*, 2003, DOI: 10.1039/b208013c, 226-227.
 - C. Stangel, C. Schubert, S. Kuhri, G. Rotas, J. T. Margraf, E. Regulska, T. Clark, T. Torres, N. Tagmatarchis, A. G. Coutsolelos and D. M. Guldi, *Nanoscale*, 2015, 7, 2597-2609.
 - A. L. M. Haffa, S. Lin, J. C. Williams, B. P. Bowen, A. K. W. Taguchi, J. P. Allen and N. W. Woodbury, *J. Phys. Chem. B*, 2004, 108, 4-7.
 - P. K. Poddutoori, A. S. D. Sandanayaka, T. Hasobe, O. Ito and A. van der Est, *J. Phys. Chem. B*, 2010, 114, 14348-14357.
 - P. K. Poddutoori, A. S. D. Sandanayaka, N. Zarrabi, T. Hasobe, O. Ito and A. van der Est, *J. Phys. Chem. A*, 2011, 115, 709-717.
 - T. Aida and S. Inoue, *Acc. Chem. Res.*, 1996, 29, 39-48.
 - G. J. E. Davidson, L. H. Tong, P. R. Raithby and J. K. M. Sanders, *Chem. Commun.*, 2006, 3087-3089.
 - Y. Hirai, T. Aida and S. Inoue, *J. Am. Chem. Soc.*, 1989, 111, 3062-3063.
 - P. P. Kumar and B. G. Maiya, *New J. Chem.*, 2003, 27, 619-625.
 - S. Richeter, J. Thion, A. van der Lee and D. Leclercq, *Inorg. Chem.*, 2006, 45, 10049-10051.
 - P. K. Poddutoori, P. Poddutoori, B. G. Maiya, T. K. Prasad, Y. E. Kandrashkin, S. Vasil'ev, D. Bruce and A. van der Est, *Inorg. Chem.*, 2008, 47, 7512-7522.
 - C. Chatterjee and M. H. Chisholm, *Inorg. Chem.*, 2011, 50, 4481-4492.
 - G. A. Metselaar, J. K. M. Sanders and J. de Mendoza, *Dalton Trans.*, 2008, DOI: 10.1039/b717017n, 588-590.
 - P. K. Poddutoori, N. Zarrabi, A. G. Moiseev, R. Gumbau-Brisa, S. Vassiliev and A. van der Est, *Chem.-Eur. J.*, 2013, 19, 3148-3161.
 - D. M. Guldi, *Chem. Commun.*, 2000, 321-327.
 - D. Guldi and N. Martin, eds., *Electron Transfer in Functionalized Fullerenes. In Fullerenes: From Synthesis to Optoelectronic Properties* Kluwer Academic Publishers, Norwell, MA, 2002.
 - M. Fujitsuka and O. Ito, in *Handbook of Photochemistry and Photobiology*, ed. H. S. Nalwa, 2003, vol. 2 Organic Photochemistry, pp. 111-145.
 - H. Imahori, K. Hagiwara, T. Akiyama, M. Aoki, S. Taniguchi, T. Okada, M. Shirakawa and Y. Sakata, *Chem. Phys. Lett.*, 1996, 263, 545-550.
 - N. Martin, L. Sanchez, B. Illescas and I. Perez, *Chem. Rev.*, 1998, 98, 2527-2547.
 - H. S. Nalwa, ed., *Photochemistry of Fullerenes. In Handbook of Photochemistry and Photobiology, vol. 2; Organic Photochemistry*, 2003.
 - F. D'Souza, P. M. Smith, M. E. Zandler, A. L. McCarty, M. Itou, Y. Araki and O. Ito, *J. Am. Chem. Soc.*, 2004, 126, 7898-7907.
 - F. D'Souza, S. Gadde, D. M. S. Islam, C. A. Wijesinghe, A. L. Schumacher, M. E. Zandler, Y. Araki and O. Ito, *J. Phys. Chem. A*, 2007, 111, 8552-8560.
 - P. A. Liddell, G. Kodis, L. de la Garza, A. L. Moore, T. A. Moore and D. Gust, *J. Phys. Chem. B*, 2004, 108, 10256-10265.
 - E. Maligaspe, N. V. Tkachenko, N. K. Subbaiyan, R. Chitta, M. E. Zandler, H. Lemmetyinen and F. D'Souza, *J. Phys. Chem. A*, 2009, 113, 8478-8489.

66. G. Kodis, Y. Terazono, P. A. Liddell, J. Andreasson, V. Garg, M. Hamburger, T. A. Moore, A. L. Moore and D. Gust, *J. Am. Chem. Soc.*, 2006, 128, 1818-1827.
67. D. Gust, T. A. Moore and A. L. Moore, *J. Photochem. Photobiol. B*, 2000, 58, 63-71.
68. Y. Kuramochi, A. Satake, M. Itou, K. Ogawa, Y. Araki, O. Ito and Y. Kobuke, *Chem.-Eur. J.*, 2008, 14, 2827-2841.
69. M. J. Frisch, G. W. Trucks, H. B. Schlegel, G. E. Scuseria, M. A. Robb, J. R. Cheeseman, G. Scalmani, V. Barone, B. Mennucci, G. A. Petersson, H. Nakatsuji, M. Caricato, X. Li, H. P. Hratchian, A. F. Izmaylov, J. Bloino, G. Zheng, J. L. Sonnenberg, M. Hada, M. Ehara, K. Toyota, R. Fukuda, J. Hasegawa, M. Ishida, T. Nakajima, Y. Honda, O. Kitao, H. Nakai, T. Vreven, J. A. Montgomery Jr., J. E. Peralta, F. Ogliaro, M. J. Bearpark, J. Heyd, E. N. Brothers, K. N. Kudin, V. N. Staroverov, R. Kobayashi, J. Normand, K. Raghavachari, A. P. Rendell, J. C. Burant, S. S. Iyengar, J. Tomasi, M. Cossi, N. Rega, N. J. Millam, M. Klene, J. E. Knox, J. B. Cross, V. Bakken, C. Adamo, J. Jaramillo, R. Gomperts, R. E. Stratmann, O. Yazyev, A. J. Austin, R. Cammi, C. Pomelli, J. W. Ochterski, R. L. Martin, K. Morokuma, V. G. Zakrzewski, G. A. Voth, P. Salvador, J. J. Dannenberg, S. Dapprich, A. D. Daniels, Ö. Farkas, J. B. Foresman, J. V. Ortiz, J. Cioslowski and D. J. Fox, Gaussian, Inc., Wallingford, CT, USA, 2009.
70. H. A. Benesi and J. H. Hildebrand, *J. Am. Chem. Soc.*, 1949, 71, 2703-2707.
71. N. Armaroli, G. Marconi, L. Echegoyen, J. P. Bourgeois and F. Diederich, *Chem.-Eur. J.*, 2000, 6, 1629-1645.
72. P. D. W. Boyd and C. A. Reed, *Acc. Chem. Res.*, 2005, 38, 235-242.
73. A. S. D. Sandanayaka, K. Ikeshita, N. Watanabe, Y. Araki, Y. Furusho, N. Kihara, T. Takata and O. Ito, *Bull. Chem. Soc. Jpn.*, 2005, 78, 1008-1017.
74. C. Luo, D. M. Guldi, H. Imahori, K. Tamaki and K. Sakata, *J. Am. Chem. Soc.*, 2000, 122, 6535-6551.
75. A. Weller, *Z. Phys. Chem.*, 1982, 133, 93-98.
76. E. A. Weiss, M. J. Ahrens, L. E. Sinks, A. V. Gusev, M. A. Ratner and M. R. Wasielewski, *J. Am. Chem. Soc.*, 2004, 126, 5577-5584.
77. O. Ito, *Res. Chem. Intermed.*, 1997, 23, 389-402.
78. T. Kato, T. Kodama, T. Shida, T. Nakagawa, Y. Matsui, S. Suzuki, H. Shiromaru, K. Yamauchi and Y. Achiba, *Chem. Phys. Lett.*, 1991, 180, 446-450.
79. Y. Araki and O. Ito, *J. Photochem. Photobiol. C-Photochem. Rev.*, 2008, 9, 93-110.
80. C. A. Reed and R. D. Bolskar, *Chem. Rev.*, 2000, 100, 1075-1119.
81. R. J. Sension, C. M. Phillips, A. Z. Szarka, W. J. Romanow, A. R. McGhie, J. P. McCauley, A. B. Smith and R. M. Hochstrasser, *J. Phys. Chem.*, 1991, 95, 6075-6078.
82. M. Fathalla, J. C. Barnes, R. M. Young, K. J. Hartlieb, S. M. Dyar, S. W. Eaton, A. A. Sarjeant, D. T. Co, M. R. Wasielewski and J. F. Stoddart, *Chem.-Eur. J.*, 2014, 20, 14690-14697.
83. O. Schalk, H. Brands, T. S. Balaban and A.-N. Unterreiner, *J. Phys. Chem. A*, 2008, 112, 1719-1729.
84. D. B. Moravec, B. M. Lovaasen and M. D. Hopkins, *J. Photochem. Photobiol. A*, 2013, 254, 20-24.
85. M. L. Kirk, D. A. Shultz, D. E. Stasiw, G. F. Lewis, G. B. Wang, C. L. Brannen, R. D. Sommer and P. D. Boyle, *J. Am. Chem. Soc.*, 2013, 135, 17144-17154.
86. A. Helms, D. Heiler and G. Mclendon, *J. Am. Chem. Soc.*, 1992, 114, 6227-6238.
87. C. Atienza, N. Martín, M. Wielopolski, N. Haworth, T. Clark and D. M. Guldi, *Chem. Commun.*, 2006, 3202-3204.
88. Y. Kandrashkin and A. van der Est, *Spectrochim Acta A*, 2001, 57, 1697-1709.